FIVE HOLE PROBE ERRORS CAUSED BY FLUCTUATING INCIDENCE

John Coull
University of Oxford
UK

Tony Dickens
University of Cambridge
UK

Henry Ng
University of Liverpool
UK

José Serna
Universidad Politécnica
de Cartagena, Spain

ABSTRACT

Steady multi-hole pressure probes are used extensively in turbomachinery research. While various sources of error are known, this paper demonstrates that fluctuations in probe incidence can be particularly damaging for accuracy.

A simple, quasi-steady model of five-hole-probe response explains why angle fluctuations can cause large errors in the indicated total and static pressure. The model explains why measurements in a shedding wake over-estimated loss by 40%. Simulated traverses behind rotors show similar behavior: fluctuating incidence causes efficiency to be under-estimated by over 1% in some cases.

The model can correct five-hole-probe errors using an estimate of unsteady flow angles. This approach reduces errors by an order of magnitude and can be used to post-correct existing test data.

1. INTRODUCTION

Many turbomachinery flows are highly three-dimensional by nature. Characterization of these flows requires the measurement of flow angles, velocity and total pressure. This is most simple to achieve using a five-hole-probe (5HP), as shown in Figure 1(a).

This paper considers "steady" 5HPs, where the probe head is connected to transducers via tubing and only averaged pressures can be measured. Steady 5HPs are ubiquitous in turbomachinery research. They are low-cost, simple to construct and easy to operate. Their small size enables intra-row traverses in rotating machines, and they are robust enough to operate in harsh environments where other measurements will fail.

"Steady" probes often experience highly unsteady flow, e.g. blade passing downstream of a rotor. The "pneumatic-averaged" data indicated by the probe will generally differ from the true time-average. It will be shown that this behavior can be largely explained using quasi-steady arguments. The analysis focuses on 5HPs, but is equally applicable to other multi-hole pneumatic probes.

1.1. Pneumatic-Averaging in Turbulent Flow

This paper will focus on large-wavelength unsteadiness, but there are parallels with previous treatments of pneumatic averaging considering small-scale turbulence.

For a pitot tube, Goldstein (1936) argued that the turbulent kinetic energy will be reversibly recovered if the eddies are small compared to the probe. Thus in incompressible flow, a pitot pointing into the flow will indicate a total pressure $\hat{P}_0$:

$$\hat{P}_0 \approx \overline{P} + \frac{\rho}{2}\overline{U}^2 + \frac{\rho}{2}\left(\overline{u^2} + \overline{v^2} + \overline{w^2}\right) = \overline{P}_0 \qquad (1)$$

where $\overline{P}$ is the time-averaged pressure, $\overline{U}$ is the mean velocity and u, v, w are the velocity fluctuation components. By these assumptions the probe indicates the true time-mean total pressure, $\overline{P}_0$.

In practice the Goldstein approximation is not always applicable. Bailey et al. (2013) compared hot-wire and pitot measurements in boundary layers,

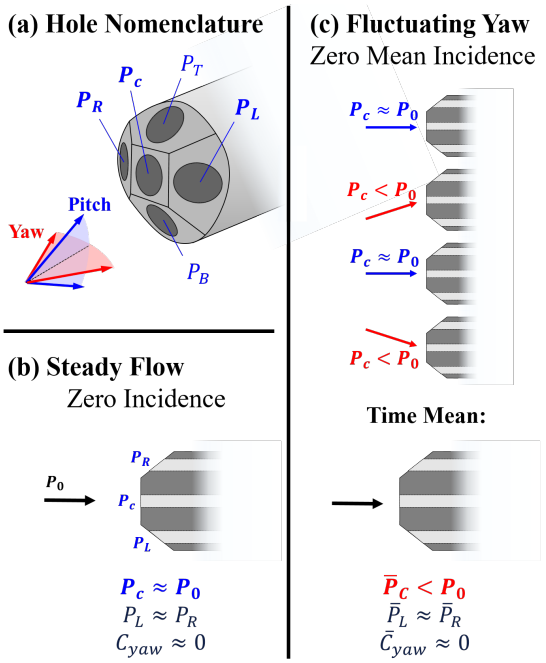

Figure 1: Five-Hole-Probe nomenclature and response in steady and fluctuating flow.

and found that only the streamwise fluctuations contributed to the indicated total pressure:

$$\hat{P}_0 \approx \overline{P} + \frac{\rho}{2}\overline{U}^2 + \frac{\rho}{2}\overline{u^2} = \overline{P}_0 - \frac{\rho}{2}\left(\overline{v^2} + \overline{w^2}\right) \quad (2)$$

Thus the pitot indicated a total pressure below the true time-mean. A similar, but greater, effect is observed in the current analysis of 5HPs.

Few authors have examined these effects for multi-hole probes. Building on the work of Bradshaw & Goodman (1968), Christiansen & Bradshaw (1981) examined yaw meters at high and low turbulence and found high static pressure errors when instantaneous yaw angles were large. This work is again consistent with the current findings.

1.2. Quasi-Steady Pneumatic-Averaging

The primary difference between true flow unsteadiness and turbulence is scale. Large-scale flow unsteadiness will affect the pressure field around the probe head. This behavior may be fundamentally unsteady, or quasi-steady, depending on the reduced frequency f_r:

$$f_r = \frac{f\,d}{V} \quad (3)$$

where f is the frequency of the fluctuation, d is the probe diameter and V is the flow velocity. A reduced frequency below ~0.3 typically indicates quasi-steady behaviour, which is found for the practical examples in this paper. At higher frequencies the behavior will begin to depart from quasi-steady behavior, but the trends are likely to be similar.

The assumption of quasi-steady flow leads to a behavior similar to equation (2). Figure 1 compares the response of a 5HP in steady flow (b), and with fluctuating yaw angle (c). In steady flow the central hole operates as a pitot and measures a pressure close to the flow total pressure, $P_C \approx P_0$.

For fluctuating yaw (Figure 1(c)) the flow is sometimes aligned with the probe and $P_C \approx P_0$. At other times there is an incidence onto the probe, so that $P_C < P_0$. Thus in the time-average, the central hole indicates a total pressure below the true time-mean of the flow, $\overline{P_C} < \overline{P}_0$.

This behavior is deeply problematic for the steady 5HP because it cannot distinguish between steady and fluctuating flow. It therefore interprets the fluctuating flow condition as simply having lower total pressure. This effect is evident in the current experiments and in the data of Bauinger et al. (2017), where 5HP measurements downstream of a turbine rotor indicated lower total pressure than Kiel-shrouded pitots.

1.3. Paper Aims and Outline

The paper aims to understand measurement errors that arise when steady 5HPs are deployed in unsteady flow. A further aim is to provide means to mitigate these errors.

Section 2 outlines the quasi-steady model. Section 3 examines how sinusoidal fluctuations affect probe errors; section 4 analyzes errors in practice, and section 5 considers strategies to mitigate and correct for the errors observed.

2. 5HP PNEUMATIC AVERAGING MODEL

2.1. Steady Flow Calibration Coefficients

Non-dimensional coefficients obtained during the steady calibration are indicated by the symbol C in this paper. For individual holes these are given by (Dominy and Hodson 1993):

$$C_X = \frac{P_X - P_0}{P_0 - P_s} \quad (4)$$

where P_0 is the flow total pressure, P_s is the static pressure and P_X is the pressure of the hole in question. The subscript X indicates the index of the hole: centre C, left L, right R, top T, bottom B, Figure 1(a). The average side-hole pressure P_{ave} is expressed as:

$$C_{ave} = \frac{P_{ave} - P_0}{P_0 - P_s} = \frac{(C_L + C_R + C_T + C_B)}{4} \quad (5)$$

Using these coefficients, the usual choice of yaw and pitch angle coefficients are:

$$C_{yaw} = \frac{P_L - P_R}{P_C - P_{ave}} = \frac{C_L - C_R}{C_C - C_{ave}} \quad (6)$$

$$C_{pit} = \frac{P_T - P_B}{P_C - P_{ave}} = \frac{C_T - C_B}{C_C - C_{ave}} \quad (7)$$

The total and dynamic pressure coefficients are typically taken as:

$$C_{P0} = \frac{P_0 - P_C}{P_C - P_{ave}} = \frac{-C_C}{C_C - C_{ave}} \quad (8)$$

$$C_{Dyn} = \frac{P_0 - P_S}{P_C - P_{ave}} = \frac{1}{C_C - C_{ave}} \quad (9)$$

Together these coefficients can also define a static pressure coefficient, here defined as:

$$C_{Ps} = \frac{P_C - P_S}{P_C - P_{ave}} = C_{Dyn} - C_{P0} = \frac{C_C + 1}{C_C - C_{ave}} \quad (10)$$

Though rarely used, it is useful for the current analysis to separate static pressure in this manner.

2.2. Probes and Calibration Ranges

For simplicity the calibration is assumed to be independent of Reynolds and Mach number. The methods can be readily extended to include these effects, which will be small for well-designed probes operating below transonic Mach numbers (<0.8).

This paper uses calibration maps from two different 5HP pyramid probes, designated as:

1) ***Grimshaw Probe*:** This probe has side faces set at **60°** from the probe axis and a diameter of 1.5mm. The calibration covers ±60° in yaw and ±20° in pitch, Grimshaw (2020).
2) ***Ng Probe*:** This probe has faces at **45°** from the probe axis and 2.2mm diameter. The calibration covers ±26° in yaw and pitch. This probe was used in the bluff body experiment (section 4.1) and by Ng and Coull (2017).

2.3. Sinusoidal Fluctuations

For the analysis in section 3, fluctuating flow is specified by defining sinusoids of arbitrary frequency. Flow angles are given by:

$$\alpha_{yaw} = \bar{\alpha}_{yaw} + A_{yaw}\, sin(t) \tag{11}$$

$$\alpha_{pit} = \bar{\alpha}_{pit} + A_{pit}\, sin\left(t + \phi_{pit}\right) \tag{12}$$

where ϕ_{pit} controls the relative phase. Fluctuating pressures can be specified relative to the *true time-mean* total ($\bar{P}_0$) and static pressure ($\bar{P}_s$) of the flow:

$$D_{P0} = \frac{P_0 - \bar{P}_0}{\bar{P}_0 - \bar{P}_s} = A_{P0}\, sin(t + \phi_{P0}) \tag{13}$$

$$D_{Ps} = \frac{P_s - \bar{P}_s}{\bar{P}_0 - \bar{P}_s} = A_{Ps}\, sin(t + \phi_{Ps}) \tag{14}$$

2.4. Quasi-Steady Probe Response

As Figure 2 shows, the instantaneous response of each hole is estimated by interpolating from the calibration map. From equation (4):

$$P_X = P_0 + C_X(P_0 - P_s) \tag{15}$$

where $C_X = f\left(\alpha_{yaw}, \alpha_{pit}\right)$ interpolates the hole calibration coefficient for the instantaneous angles. Normalized by the time-mean flow, the dynamic (i.e. instantaneous) pressure coefficients are thus:

$$D_X = \frac{P_X - \bar{P}_0}{\bar{P}_0 - \bar{P}_s} = D_{P0} + C_X(D_{P0} - D_{Ps} + 1) \tag{16}$$

2.5. Pneumatically-Averaged Response

Pneumatic averaging is modelled by time-averaging each hole pressure, giving the following pitch and yaw coefficients:

$$\hat{C}_{yaw} = \frac{\bar{D}_L - \bar{D}_R}{\bar{D}_C - \bar{D}_{ave}} \tag{17}$$

$$\hat{C}_{pit} = \frac{\bar{D}_T - \bar{D}_B}{\bar{D}_C - \bar{D}_{ave}} \tag{18}$$

These *probe-indicated* values are denoted using over-hats, and may differ from the true time average of the instantaneous coefficients, $\bar{C}_{yaw}$ and $\bar{C}_{pit}$.

Indicated angles are calculated by interpolating from the calibration map in typical fashion:

$$\hat{\alpha}_{yaw}, \hat{\alpha}_{pit} = f\left(\hat{C}_{yaw}, \hat{C}_{pit}\right) \tag{19}$$

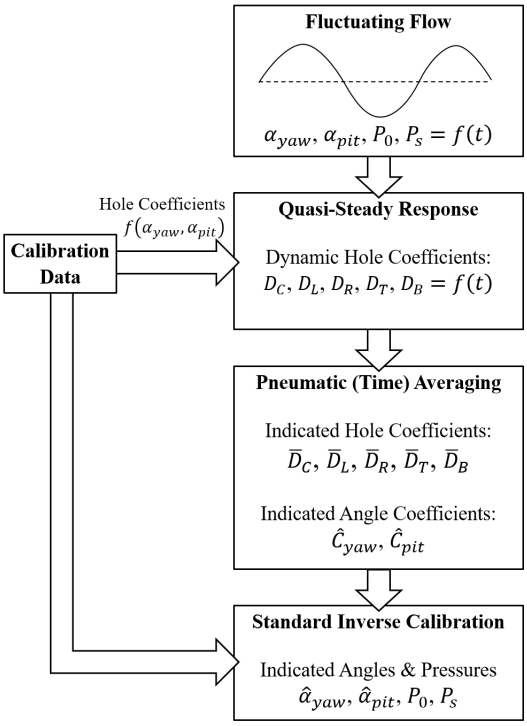

Figure 2: Quasi-Steady model.

The errors from the true time mean flow angles are:

$$E_{yaw} = \hat{\alpha}_{yaw} - \bar{\alpha}_{yaw} \tag{20}$$

$$E_{pit} = \hat{\alpha}_{pit} - \bar{\alpha}_{pit} \tag{21}$$

The indicated total and dynamic pressure coefficients are interpolated from the calibration using the indicated angles:

$$\hat{C}_{P0}, \hat{C}_{Ps}, \hat{C}_{Dyn} = f\left(\hat{\alpha}_{yaw}, \hat{\alpha}_{pit}\right) \tag{22}$$

Again these values may differ from the true time averages. Non-dimensional errors in the indicated total, dynamic and static pressure, are then defined relative to the true time-average flow:

$$E_{P0} = \frac{\widehat{P_0} - \bar{P}_0}{\bar{P}_0 - \bar{P}_s} = \bar{D}_C + \hat{C}_{P0}(\bar{D}_C - \bar{D}_{ave}) \tag{23}$$

$$E_{Ps} = \frac{\widehat{P_s} - \bar{P}_s}{\bar{P}_0 - \bar{P}_s} = 1 + \bar{D}_C - \hat{C}_{Ps}(\bar{D}_C - \bar{D}_{ave}) \tag{24}$$

$$E_{Dyn} = \frac{\widehat{P_0} - \widehat{P_s}}{\bar{P}_0 - \bar{P}_s} - 1 = \hat{C}_{Dyn}(\bar{D}_C - \bar{D}_{ave}) - 1 \tag{25}$$

Each error is positive when the quantity is over-estimated by the probe and vice-versa. For steady flow all errors are zero by definition.

3. SINUSOIDAL FLOW FLUCTUATIONS

3.1. Angle Fluctuations in One Component

For the Grimshaw probe, Figure 3 shows the response to a sinusoidal fluctuation of ±25° in yaw angle, for zero mean incidence. The instantaneous points simply follow the calibration line for $\alpha_{pit} = 0$. Because the calibration is *anti-symmetric* and

almost linear, positive and negative incidence effects tend to cancel each other. Thus the pneumatic average Yaw Coefficient $\hat{C}_{yaw}$ is close to zero, and the probe indicates a yaw angle $\hat{\alpha}_{yaw} \approx 0$.

Figure 4 shows the total pressure response for the same fluctuation. In contrast to yaw angle, C_{P0} vs α_{yaw} is highly non-linear and *symmetric*: both positive and negative yaw cause the central hole pressure to drop. This effect is illustrated schematically in Figure 1(c). As a result, the time-average total pressure coefficient (equation (8)) is greater than zero, $\bar{C}_{P0} \approx 0.2$. This value is the correction that *should* be applied to the central hole to give the correct flow total pressure.

In the absence of knowledge of fluctuations, the 5HP must use the indicated flow angles ($\hat{\alpha}_{yaw} \approx 0$, $\hat{\alpha}_{pit} \approx 0$) to interpolate for C_{P0} from the steady calibration data. The steady data gives a total pressure coefficient $C_{P0} = 0.01$, and thus the probe indicates a lower total pressure than the true value.

In general the calibration map for static pressure has a similar shape and symmetric response to angle as for total pressure. However the behavior and response depends on the probe design. Figure 5 shows the static pressure response for the Grimshaw probe. Because of its high face angle (60°), the static pressure coefficient is relatively insensitive to angles over this range. Thus the underestimation of P_s in Figure 5 is only around $0.04(P_C - P_{ave})$. Figure 6 shows the response of the Ng probe, which has face angles of 45° and is more sensitive to angle. As shown, this results in static pressure being underestimated by $0.37(P_C - P_{ave})$.

3.2. Angle Fluctuations in Two Components

Single-component angle fluctuations are unlikely in practice. Figure 7 therefore shows the total pressure errors for a range of values of A_{yaw}, A_{pit} and phase ϕ_{pit} for the two probes. The effect of phase is minimal and the errors collapse to a function of the compound angle, in radians:

$$E_{P0} \approx -0.8\left(A_{comp}\right)^{2.3} \tag{26}$$

where the compound angle fluctuation is given by:

$$A_{comp} = \sqrt{A_{yaw}^2 + A_{pit}^2} \tag{27}$$

This result reflects the approximately symmetric probe response to yaw and pitch. Figure 7(a) includes the Bailey et al. pitot correction from equation (2) applied to the central hole. In general the Bailey approach is accurate for small incidence (<20°) but underestimates the error for high instantaneous yaw angles.

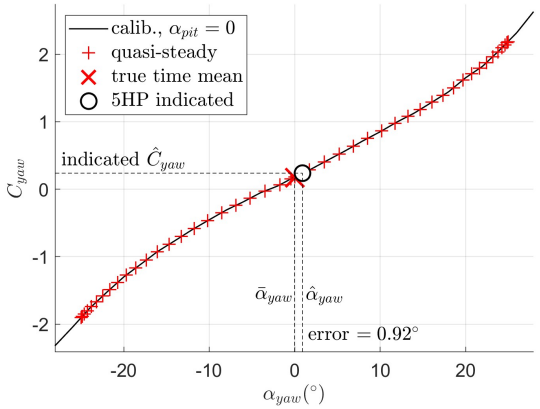

Figure 3: Yaw Angle response to ±25° fluctuating Yaw, Grimshaw Probe.

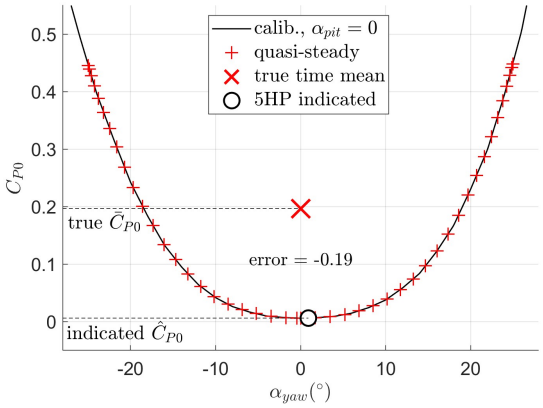

Figure 4: Total Pressure response to ±25° fluctuating Yaw, Grimshaw Probe.

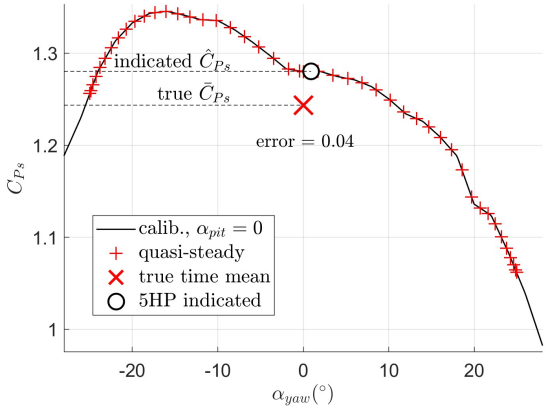

Figure 5: Static Pressure response to ±25° fluctuating Yaw, Grimshaw Probe.

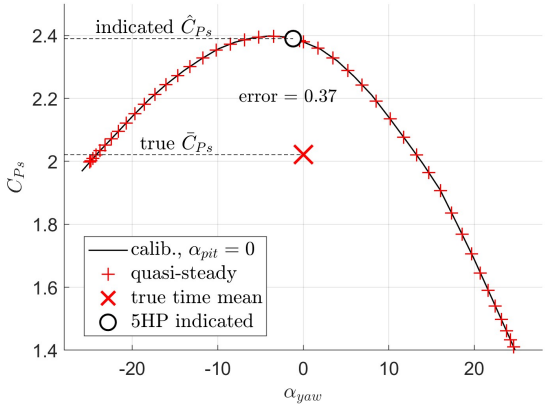

Figure 6: Static Pressure response to ±25° fluctuating Yaw, Ng Probe.

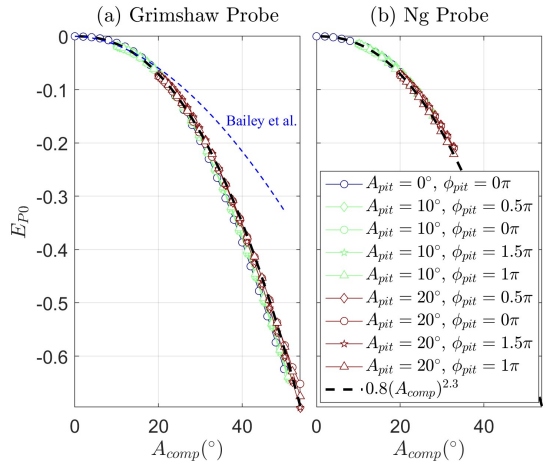

Figure 7: Total Pressure Errors for fluctuating yaw and pitch; A_{yaw} increasing from left to right.

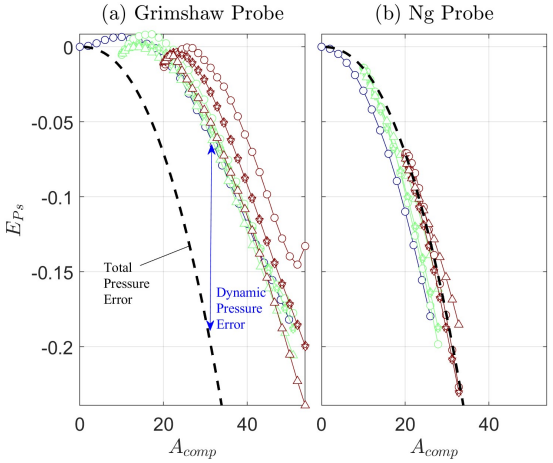

Figure 8: Static Pressure Errors for fluctuating yaw and pitch, legend in Figure 7.

The static pressure errors are presented in Figure 8 (note the difference in scale). As before the two probes respond differently but the results approximately collapse to give $E_{Ps} \approx f(A_{comp})$. The scatter is greater than for total pressure, reflecting the poorer conditioning of the static pressure measurement, e.g. Dominy and Hodson (1993). The static pressure coefficient C_{Ps} is also less directionally symmetric (Figure 5, Figure 6) than the total pressure coefficient.

Figure 8 also compares the static-to-total errors. As can be seen this determines the resultant dynamic pressure error. The Grimshaw probe (Figure 8(a)) has lower static errors due to its sharp face angles, but therefore underestimates dynamic pressure. In contrast the Ng probe (Figure 8(b)) has similar total and static pressure errors and therefore has much lower dynamic pressure error.

3.3. The Effect of Mean Incidence

Figure 9 shows pressure errors as the time-averaged yaw angle ($\bar{\alpha}_{yaw}$) is varied for a yaw angle fluctuation of ±25°. In general having a mean angle

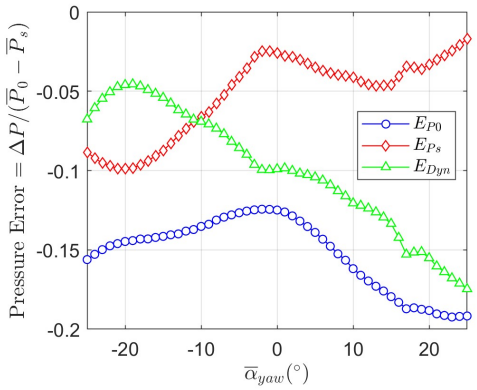

Figure 9: Pressure Errors vs. mean yaw angle with $A_{yaw} = \pm 25°$, Grimshaw probe.

close to zero (as in "nulled operation") tends to slightly reduce errors, because the calibration map gradients tend to be lower close to zero incidence.

3.4. Comments on Pressure Fluctuations

For fluctuations in pressure only, the model predicts zero error: for fixed flow angles each hole coefficient C_X is constant and thus equation (16) is linear to D_{P0} and D_{PS}. However when combined with changes in angle, certain phases of pressure perturbation were found to increase or decrease error depending on the phase. These effects are driven by the covariance of angle and pressure, which introduces biases in the pneumatic averaging. However in most cases these pressure fluctuation effects were small, and were negligible in the practical cases discussed in the following section.

4. FLUCTUATION ERRORS IN PRACTICE

This section examines two typical measurement set-ups where fluctuating probe incidence may be experienced. The first considers shedding wakes; the second considers turbomachinery traverses affected by blade-passing unsteadiness.

4.1. Shedding Wakes

Measurements were obtained with the Ng probe in the midspan wake of a D-shaped bluff body in an enclosed wind tunnel, as shown in Figure 10. The Reynolds number is 98,500 based on the body width W and upstream velocity V_∞. The ratio of span to width is 4.8, tunnel blockage is 12% and Mach < 0.1.

The probe reduced frequency (equation (3)) can be related to the Strouhol number ($St = fW/V_\infty$) of the oscillations:

$$f_r = \frac{f\,d}{V} = St\frac{V_\infty}{V}\frac{d}{W} \qquad (28)$$

The upstream-to-wake velocity ratio V_∞/V varies between about 0.9 and 1.4, and the probe diameter is small relative to the trailing edge ($d/W < 0.03$). For the primary shedding frequency ($St = 0.2$) the reduced frequency is therefore less than 0.01 and the probe response will be quasi-steady.

The symbols in Figure 11 show experimental measurements. Figure 11(a) compares the total pressure loss from the 5HP and a Kiel-pitot. The Kiel is insensitive to angle over the range ±30° so has minimal fluctuating angle error. The 5HP indicates erroneous losses which are 44% higher at the wake centerline. Figure 11(b) compares static pressure from the 5HP with values from a row of static tappings on the tunnel sidewall. In the wake centerline the 5HP indicates a much lower pressure, by around 30% of the freestream dynamic head.

To aid analysis, an Unsteady Reynolds-Averaged-Navier-Stokes (URANS) calculation was performed with Fluent (v18.2). The Scale-Adaptive-Simulation turbulence model of Menter and Egorov (2010) was used. The mesh has approximately 4M cells and uses wall functions to resolve the boundary layer. Approximately 100 timesteps were used for each fundamental shedding cycle, and data were collected for 20 cycles after transients. Figure 11(a) shows that the predicted time-average total pressure loss is nearly identical to the Kiel measurements. Sidewall static pressure is close to the tapping data, and lower pressure (higher C'_{Ps}) is predicted in the wake centerline at midspan, shown in Figure 11(b).

The URANS calculation gives a direct estimate of the unsteady flow experienced by the 5HP in the experiment. Figure 12 shows time traces of angles at the centerline of the wake. Yaw oscillations (within the plane of Figure 10) of ±35° are observed with smaller variation in pitch (typically ±15°). This gives a compound angle (A_{comp}, equation (27)) of around ±40°. Equation (26) and Figure 7 therefore suggest a total pressure error of around 35%.

A more accurate quantification is obtained by directly inputting the time series of flow angle and pressure into the quasi-steady model. The angles exceed the range of the calibration (±26°), and the map was therefore extended by linearly extrapolating individual hole coefficients. This introduces only small uncertainty since similar results were obtained by limiting the flow angles.

The predicted response of the 5HP is shown in Figure 11. The model mimics the measurement errors observed, predicting a 40% error in loss and 20% error in non-dimensional static pressure. Figure 11 also includes predictions of probe response using *only the angle fluctuations* i.e. ignoring total and static pressure fluctuations. This gives nearly identical results, confirming that it is the angle fluctuations that cause the error. Figure 13 demonstrates that pressure fluctuations are not strongly correlated with the yaw angle fluctuations, which is why they have little influence.

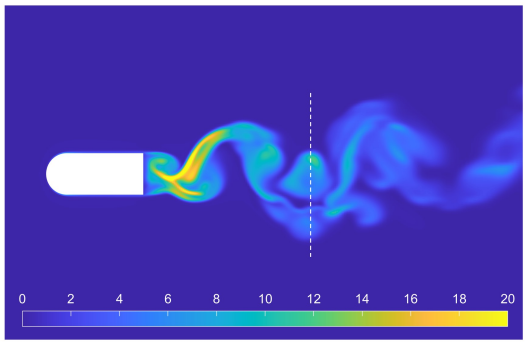

Figure 10: Instantaneous Turbulent Kinetic Energy in the midspan plane (URANS). Dashed line indicates traverse plane.

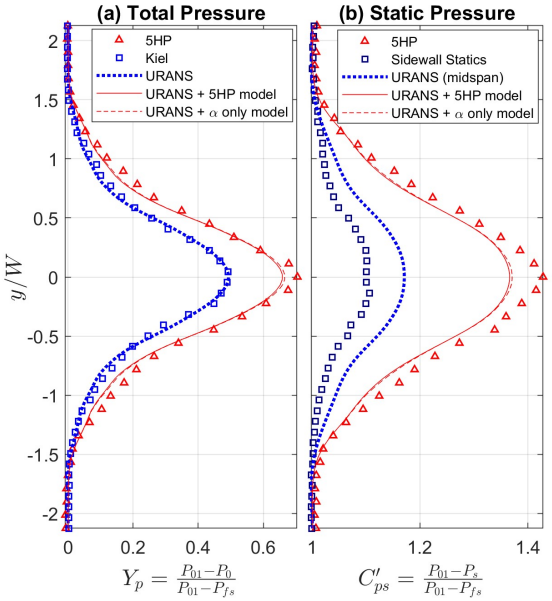

Figure 11: Total and Static Pressure in the midspan wake of a D-shaped bluff body, Ng Probe. P_{01} is the inlet total pressure; P_{fs} is static pressure at the edge of the wake.

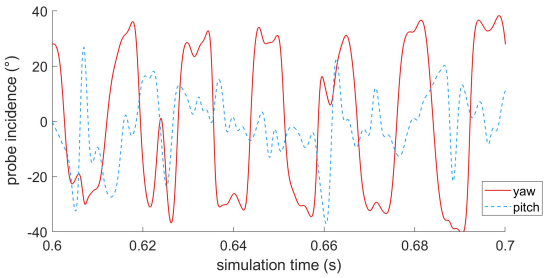

Figure 12: Angles at the wake centerline.

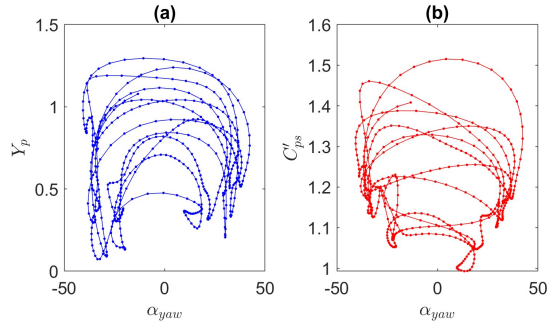

Figure 13: (a) total and (b) static pressure correlation with yaw angle, wake centerline.

4.2. Stationary-Frame Traverses behind a Rotor

Turbine efficiency measurements require knowledge of flow conditions downstream of the rotor. Due to small inter-stage gaps or access restrictions, traverse planes are often close to the rotor blade trailing edge. The spatial non-uniformity in the relative frame will therefore be experienced as a *time-varying* flow by a stationary probe. The reduced frequency for the blade-passing is:

$$f_r = \frac{\cos \alpha_2}{\phi}\left(\frac{d}{s}\right) \qquad (29)$$

where s is pitch, α_2 is the rotor exit angle in the absolute frame, and ϕ is the flow coefficient. Typically $(\cos \alpha_2 / \phi) < 2$, and the response will be quasi-steady provided the probe diameter d is small relative to the blade pitch ($d/s < 0.15$).

A 5HP traverse of the Grimshaw probe is simulated by extracting data from a Reynolds-Averaged-Navier-Stokes (RANS) calculation of a High Pressure Turbine rotor with a squealer tip. Details are given in Coull et al. (2014). A radial traverse plane is taken close to the trailing edge (first plane in Figure 15), at an axial distance of about 5% of chord at the hub to around 15% at the tip. The unsteady flow experienced by the probe is calculated by accounting for the change of reference frame.

Figure 14 illustrates the mean and peak-to-peak probe incidence for two set-ups: (1) with fixed probe yaw angle; and (2) nulling the probe at each height to minimise incidence. The flow fluctuations are small at midspan (around ±10°) but much larger in the endwall regions. The instantaneous flow angles are limited to the calibration range of the Grimshaw probe, indicated in Figure 14, and so pressure errors are likely to be slightly underestimated.

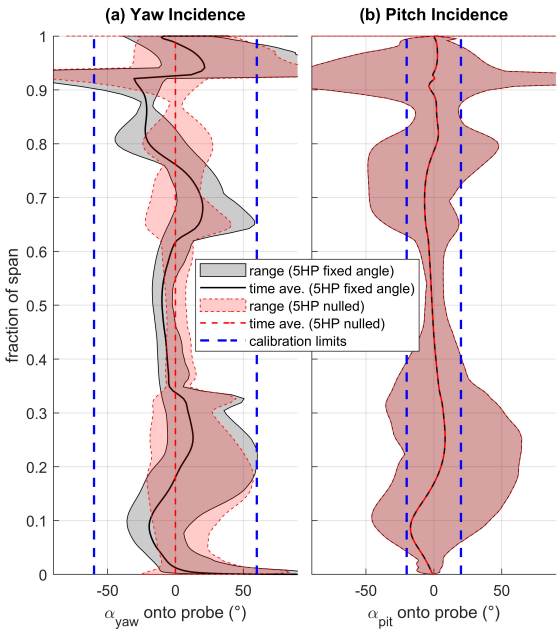

Figure 14: Predicted probe angle fluctuations.

Predicted traverse results are shown in Figure 16; the pressures coefficients are defined using the true mass-averaged total and static pressures in the absolute frame. Integrated values for each virtual measurement are compared in Table 1.

One must first note that an "ideal" probe will perfectly time-average the flow at each height, and does not measure the mass-average. As the symbols in Figure 16 show, this causes significant discrepancy in the region of the tip leakage flow (>90% of span). Table 1 shows that the time-averaged Y_p is around 2% higher than the mass-average, leading to an under-estimation of efficiency by around 0.4%.

The lines on Figure 16 show the estimated 5HP response. Only the fluctuating angles have been considered since pressure fluctuations had minimal effect. At midspan where the fluctuations are small the errors are relatively low ($\Delta Y_p < 1\%$). However in the endwall regions Y_p is over-estimated by as much as 30%, and static pressure by 5-10%. (Much larger static pressure errors would be experienced with the Ng probe.) These results are in agreement with Bauinger et al. (2017), who found that a 5HP downstream of a rotor measured lower total pressure than a Kiel. Their under-estimation was more severe in the tip region where flow angle fluctuations tend to be greatest.

	True Mass average	True Time average	5HP fixed angle	5HP nulled
normalised $\dot{m}$	1	0.97	0.90	0.90
$\Delta\bar{Y}_p$	0	+2.1%	+10.6%	+9.7%
$\Delta\bar{C'}_{ps}$	0	+0.0%	+1.4%	+0.6%
$\Delta\bar{\alpha}_{yaw}$	0	-0.2°	+0.8°	+0.6°
$\Delta\bar{\alpha}_{pit}$	0	+0.1°	+1.3°	+1.1°
$\Delta\eta$	**0**	**-0.35%**	**-1.52%**	**-1.42%**

Table 1 : Integrated errors for near-plane traverse (Figure 14), Grimshaw probe.

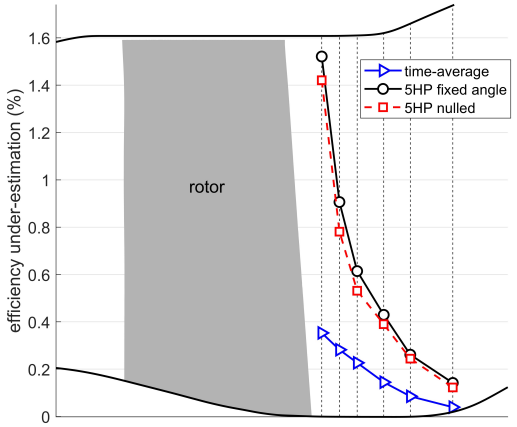

Figure 15: Predicted Efficiency Errors for different traverse planes, Grimshaw probe.

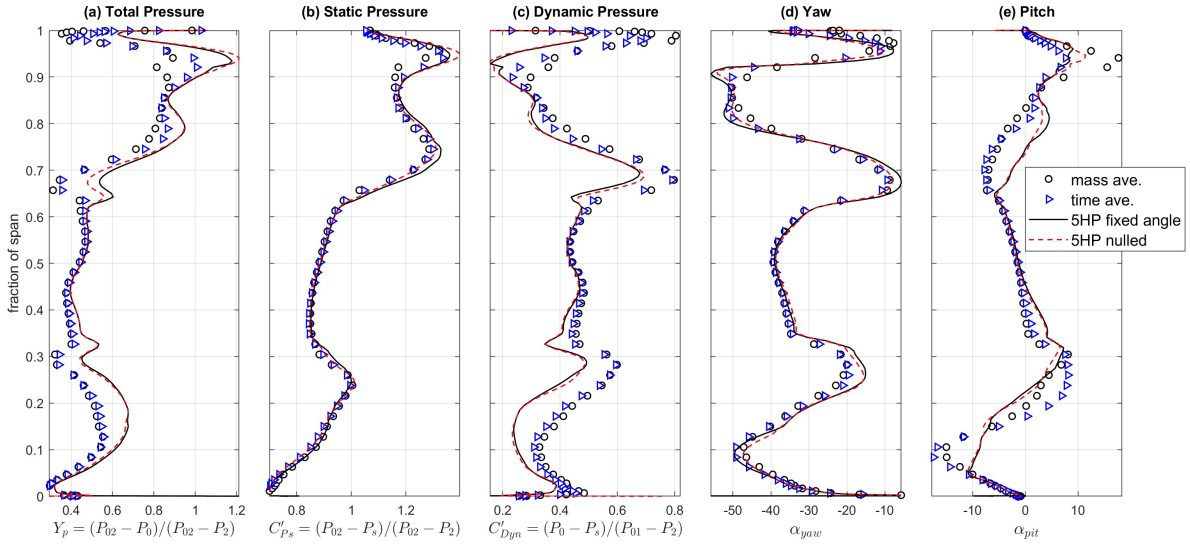

Figure 16: Simulated 5HP Traverse downstream of turbine rotor, Grimshaw probe. Instantaneous angles limited to ±60° in yaw and ±20° in pitch.

Table 1 details the errors in the calculated mass-averages. The fixed-angle 5HP indicates a rotor efficiency 1.5% below the true mass-average, which can be improved slightly to 1.4% by nulling the probe at each height. On top of the time-averaging effects, the fluctuating angles cause an error of at least 1.1%. This error is much larger than the accuracy typically quoted for such experiments. Figure 15 shows that the errors decrease if the traverse plane is moved downstream, where the flow becomes more uniform and the fluctuations reduce. To achieve an efficiency error below 0.2% requires around one axial chord distance from the trailing edge, which will not be feasible in many cases.

This exercise was repeated for a research compressor. Traverse data obtained 10% of an axial chord downstream of a stator were used to simulate an equivalent rotor in the relative frame. The predicted angle fluctuations were generally larger at midspan than the turbine (Figure 14), but much smaller at the endwalls. The predicted efficiency under-prediction was therefore smaller but still significant, at around 0.7% (of which 0.2% was due to time- vs. mass-averaging).

5. MITIGATION STRATEGIES

The results suggest that several past and present measurement set-ups may be corrupted by angle fluctuation errors. This has implications for turbomachinery efficiency measurements and the validation of numerical methods. This section therefore considers practical steps to (1) identify potential errors; (2) correct existing data; and (3) minimize angle fluctuation errors in the first place.

5.1. Identifying and Assessing Error Magnitude

An attempt was made to identify errors by examining the departure of individual holes from the calibration data, e.g. as proposed by Yasa and Paniagua (2012). This approach was found to be unreliable because some combinations of pitch and yaw fluctuation produce the same response as steady flow. This method may be more successful for probes with more than five holes.

The correction recommended is therefore to obtain an estimate of angle fluctuations for each set-up. In some cases this will be possible to measure, e.g. using cross-wires or Laser Doppler Anemometry. In other cases an estimate can be generated computationally or analytically. The error predictions for sinusoidal fluctuations (e.g. equation (26), Figure 7 and Figure 8) can be then used to give a first estimate of likely errors.

5.2. Error Correction

When a significant error is anticipated, the quasi-steady model can be used to correct 5HP data. The precision of this correction depends on (1) the accuracy of estimated flow angle fluctuations, and (2) having sufficient angle range on the calibration. If a wide calibration range is not available for the probe in question, linear extrapolation or a calibration for a similar probe could be used instead. As shown, the static pressure correction will be most sensitive to the details of probe geometry.

Figure 17 illustrates this approach for the bluff body data in section 4.1. The 5HP-indicated-values have been corrected using the URANS predictions of fluctuating angles. The method corrects for around 80-90% of the errors in total and static pressure. Table 2 shows calculated drag coefficients based on upstream conditions. Form drag dominates over viscous drag, so the drag coefficient $C_D = 0.74$ from integration of surface static pressures should be reasonably accurate. The URANS wake data agrees within 3%. The Kiel combined with sidewall statics

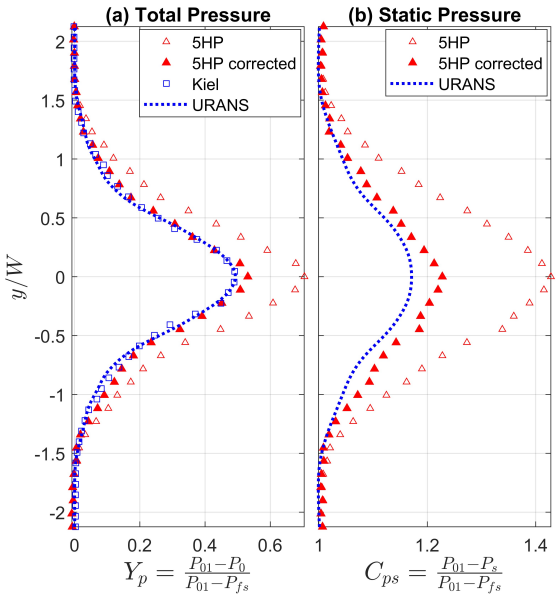

Figure 17: Correction of 5HP data for the bluff body using URANS flow angles.

	Surface Static Tappings	URANS	Kiel + sidewall statics	5HP indicated	5HP corrected
C_D	0.74	0.72 -2.7%	0.70 -5.7%	**1.31** **+76%**	**0.80** **+7.7%**

Table 2 : Indicated Drag Coefficients for the bluff body.

underestimate drag by 6% because the midspan static pressure is lower than the sidewall (see Figure 11(b)). The 5HP overestimates drag by 76%, but the correction reduces this error to less than 8%.

For traverses downstream of rotors, a correction for mass- vs. time-averaging (Figure 15) should also be performed. This is equivalent to pitch-wise mass- vs. area-averaging in the relative frame.

5.3. Designing-Out Error

Finally, it is useful to consider how angle fluctuation errors can be designed out of experiments. Several observations can be made:

- Kiel-pitots should be used to cross-check 5HP data when fluctuations may be present.
- Traverse planes behind rotors should be as far downstream as possible to minimise error.
- Alternatively, these traverses could be performed with probes mounted in the rotating frame to remove the blade passing fluctuations.
- Pneumatic averaging errors can be avoided completely by use of fast-response multi-hole probes. More work is needed to miniaturise such probes to improve spatial accuracy.
- Fast-response single-hole probes can be used as virtual three-hole-probes by locking to the rotor passing (e.g. Lenherr et al. 2011). This approach accounts for periodic yaw angle fluctuations which will be the largest source of error, but further work is required to assess the residual error due to the unresolved fluctuating angles.

Errors could also be minimised with new multi-hole probes with low angle sensitivity for total and static pressure. For example a hybrid 5HP with a Kiel-pitot central hole would be much less prone to errors. Challenges remain to develop, characterise and miniaturise such probes.

6. CONCLUSIONS

A simple quasi-steady analysis of 5HP response in unsteady flow has demonstrated that angle fluctuations can cause large errors in indicated total and static pressure.

For zero incidence and steady flow, the central hole reads close to the flow stagnation pressure. However when angles fluctuate about a zero mean, the central hole experiences a lower pressure for *both* positive and negative incidence. As a result the probe underestimates total pressure for fluctuating angles. This mechanism was shown to cause up to 40% error in loss coefficient in the unsteady wake of a bluff body. For a simulated traverse in the stationary-frame downstream of a turbine rotor, the unsteady angles cause efficiency to be underestimated by more than 1%.

Static pressure suffers similar errors but the magnitude depends on the probe design. The errors are smaller for probes with more swept-back side faces because they are less sensitive to angle.

The findings suggest that fluctuating angle errors may have corrupted a significant body of research data, in particular for turbine efficiency measurements. The model offers a means to back-correct existing data, using an estimate of the fluctuating incidence angles onto the probe. This approach reduced errors by an order of magnitude in the case of the bluff body.

Ideally, 5HP data should be corroborated with Kiel-pitot measurements whenever significant fluctuating flow angles may be present.

ACKNOWLEDGEMENTS

The authors would like to thank Rolls-Royce for funding and permission to publish, with particular thanks to Dr Raul Vazquez and Dr Duncan Simpson. Prof Luca di Mare, University of Oxford, provided advice on the URANS calculation set-up. Dr Sam Grimshaw of the Whittle Laboratory, University of Cambridge, provided a sample calibration map.

REFERENCES

Bailey, S.C.C., Hultmark, M., Monty, J.P., Alfredsson, P.H., Chong, M.S., Duncan, R.D.,

Fransson, J.H.M., Hutchins, N., Marusic, I., McKeon, B.J., Nagib, H.M., Örlü, R., Segalini, A., Smits, A.J., and Vinuesa, R., 2013, "Obtaining Accurate Mean Velocity Measurements in High Reynolds Number Turbulent Boundary Layers Using Pitot Tubes," *J. Fluid Mech.*, 715, pp. 642–670

Bauinger, S., Marn, A., Göttlich, E. and Heitmeir, F., 2017. Influence of pressure fluctuations on the mean value of different pneumatic probes. *International Journal of Turbomachinery, Propulsion and Power*, 2(3), p.13.

Bradshaw, P. & Goodman, D.G. 1968 The effect of turbulence on static-pressure tubes. *Reports and Memoranda 3527. Aeronautical Research Council*.

Christiansen, T. & Bradshaw, P. 1981 Effect of turbulence on pressure probes. *Journal of Physics E: Scientific Instruments* 14 (8), 992–997

Dominy, R.G. and Hodson, H.P., 1993. An investigation of factors influencing the calibration of five-hole probes for three-dimensional flow measurements. *Journal of Turbomachinery,* 115(3), pp.513-519.

Coull, J.D., Atkins, N.R., and Hodson, H.P., 2014, High-Efficiency Cavity Winglets for High Pressure Turbines, *ASME Turbo Expo 2014: Turbomachinery Technical Conference and Exposition.*

Goldstein, S., 1936. A note on the measurement of total head and static pressure in a turbulent stream. *Proceedings of the Royal Society of London. Series A-Mathematical and Physical Sciences,* 155(886), pp.570-575.

Grimshaw, S.D., 2020, private communication

Lenherr, C., Kalfas, A.I. and Abhari, R.S., 2011. High temperature fast response aerodynamic probe. *Journal of Engineering for Gas Turbines and Power*, *133*(1), p.011603.

Menter, F.R. and Egorov, Y., 2010. The scale-adaptive simulation method for unsteady turbulent flow predictions. Part 1: theory and model description. *Flow, Turbulence and Combustion*, *85*(1), pp.113-138.

Ng, H.C.H. and Coull, J.D., 2017. Parasitic loss due to leading edge instrumentation on a low-pressure turbine blade. *Journal of Turbomachinery*, *139*(4)

Yasa, T. and Paniagua, G., 2012. Robust procedure for multi-hole probe data processing. *Flow Measurement and Instrumentation*, *26*, pp.46-54.